Optics & Laser Technology 180 (2025) 111499

Contents lists available at ScienceDirect

Optics and Laser Technology

journal homepage: www.elsevier.com/locate/optlastec

Full length article

Thermal analysis of diode-pumped femtosecond-laser-written Pr:$LiLuF_4$ waveguide lasers

Davide Baiocco [a,*], Ignacio Lopez-Quintas [b], Javier R. Vázquez de Aldana [b], Mauro Tonelli [a], Alessandro Tredicucci [a]

[a] Dipartimento di Fisica, Università di Pisa, Largo Bruno Pontecorvo 3, Pisa, 56127, Italy
[b] Grupo de Investigación en Aplicaciones del Láser y Fotónica, Universidad de Salamanca, Pl. La Merced SN., Salamanca, 37008, Spain

ARTICLE INFO

Keywords:
Praseodymium
Visible laser
Waveguide laser
Direct femtosecond writing

ABSTRACT

In this work we report a thermal stress test executed on high efficiency diode pumped waveguide lasers based on Pr:$LiLuF_4$. Numerical simulations have been performed to estimate the core temperature. We demonstrated that no modifications in the output power, 275 mW at 604 nm and 310 mW at 721 nm, and in the bulk-level slope efficiency, 40% at 604 nm and 50% at 721 nm, have been observed with an estimated core temperature of 70 °C. We also executed stability measurements of the free running laser in thermally severe conditions, demonstrating output power fluctuations of mechanical origin as low as 10% of the peak value.

1. Introduction

From the first works of Davis [1], direct femtosecond laser writing was employed to realize guiding structures in many materials [2]. By irradiating the sample with ultrashort laser pulses, it is possible to permanently modify the refractive index of the irradiated material and create waveguides. This technique has been employed for the construction of compact solid state lasers (SSLs). By building waveguide devices, it is possible to exploit in more practical settings the intrinsic temporal stability and reduced emission bandwidth of SSLs, crucial features in metrological devices. Moreover, the typical high quality beam of SSLs facilitates the inclusion of this type of sources in complex optical systems. On the contrary, laser diodes, although allowing electrical pumping, suffer from frequency runaway [3] and have an emission characterized by a high M^2. In the last years, many works have been published describing the fabrication of waveguide lasers operating in the wavelength range of 1 μm–3 μm, using erbium [4], neodymium [5,6], thulium [7,8], or ytterbium [9] as dopant in the active medium.

Fabricating waveguide lasers directly operating in the visible range requires high quality materials and waveguides with low propagation losses in that spectral region. An interesting ion for direct visible lasing is praseodymium. The Pr^{3+} ion possesses emission lines in all the visible range, from the cyan emission at 480 nm, to the green transitions at 520 nm and 540 nm, the orange one at 604 nm, the 640 nm in the red region, and the two in the deep red, at 698 nm and 721 nm. Moreover, it has been demonstrated that it is possible to make praseodymium based lasers working on all the lines necessary for the operation of the atomic clock based on the neutral strontium atom [10], and lasers based on Pr^{3+} can also be applied in the medical field [11]. Such lasers have been intensively studied after the development of Watt-level InGaN-based laser diodes [12,13], which constitute a compact and inexpensive pump source for praseodymium ions, due to their absorption around 445 nm, given by the presence of the $^3H_4 \rightarrow {}^3P_2$ absorption transition.

Among various materials tested as host for Pr^{3+} ions, the best performances have been achieved with fluoride crystals. In fact, fluoride crystals stand out for their lower crystal field effect and a lower effective phonon energy. The first feature reflects in a greater energy splitting between the $^3P_2$ manifold and the lowest 4f5d levels, that prohibits excited state absorption at the laser and the pump wavelengths, while the second reduces the phonon mediated nonradiative decay of the upper laser level. Moreover, these single crystals are chemically stable and not hygroscopic, both interesting properties in the framework of long term applications and chemically severe environments. Contrary to what happened in the infrared region, in the last years only a few works regarding Pr-based waveguide lasers have been published [14–22]. In addition, guiding structures have been demonstrated in Pr:YAG [23].

The aim of this work is to demonstrate the possibility of operating an all-solid state, high-efficiency, diode-pumped, Pr-based waveguide laser in high temperature conditions, without affecting the output power delivered from the system and its slope efficiency. We also checked the stability of the system in these severe conditions, to test the

* Corresponding author.
E-mail address: davide.baiocco@phd.unipi.it (D. Baiocco).

https://doi.org/10.1016/j.optlastec.2024.111499
Received 27 May 2024; Received in revised form 4 July 2024; Accepted 17 July 2024
Available online 26 July 2024

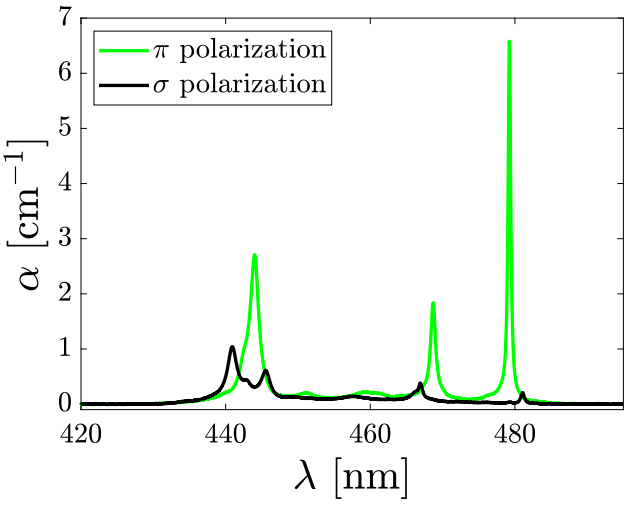

Fig. 1. Absorption spectra of Pr:LLF.

feasibility of implementing a waveguide system in a possible monolithic device. The choice of employing a laser diode as pump source is due to its greater compactness, stability and lower cost with respect to other commercially available pump sources like 2ω-OPSL lasers [24]. Moreover, it has been demonstrated that it is possible to obtain bulk-level slope efficiencies with this type of pump sources [22].

2. Material growth and waveguide inscription

The crystal matrix we chose for our work is $LiLuF_4$ (LLF). LLF is a tetragonal crystal (a = 5.1 Å, c = 10.5 Å) [19], isomorph to the scheelite and to $LiYF_4$ (YLF). With respect to YLF, LLF shows better thermomechanical properties [25], as a more uniform thermal conductivity, can be grown from a congruent melt, facilitating the growth of high quality crystals, and possesses a lower effective phonon energy [26]. In LLF, the $^3H_4 \rightarrow {}^3P_2$ absorption transition lies at 444 nm, and the lifetime of the $^3P_0$ level is about 45 µs [27]. The crystal is birefringent and, in particular, uniaxial, due to its tetragonal structure. The difference in refractive index between the ordinary index and the extraordinary one is about 0.02 in all the visible range. The tetragonal structure reflects also in the fluorescence spectrum being different for π-polarized light (E//c) and σ-polarized light (E//a) [27]. When embedded in LLF, the transitions of Pr^{3+} with the highest emission cross section are located at 480 nm (197×10^{-21} cm^2), 604 nm (93×10^{-21} cm^2) and 721 nm (72×10^{-21} cm^2) for π-polarization, while main lines for σ-polarization are at 607 nm (118×10^{-21} cm^2) and 640 nm (210×10^{-21} cm^2). The complete fluorescence spectrum, together with the emission cross section of all lines are reported in [12].

Pr-doped LLF was produced by Czochralski method at the University of Pisa from high-purity powders of the constituents: LiF, LuF_3 and PrF_3, provided by AC Materials (Tarpon Springs, FL, USA). The dopant concentration in the melt was of 1%. The as-grown boule was oriented by X-ray backscattering Laue technique to cut a sample with oriented facets, due to the anisotropic nature of the crystal matrix. Owing to segregation effects [27], the actual praseodymium concentration is lower than that found in the melt. We estimated the concentration by acquiring polarized absorption spectra with a CARY 5000 spectrophotometer (Fig. 1, resolution 0.09 nm), and comparing the absorption coefficient with the absorption cross sections available in the literature [12]. The estimated value for the actual dopant concentration is 0.2%. Consequently, we carved a sample with dimensions 4 mm(a) × 4 mm(c) × 9 mm(a) in order to write 9 mm-long waveguides.

The procedure for the waveguide fabrication was the direct irradiation with femtosecond laser pulses generated in an amplified

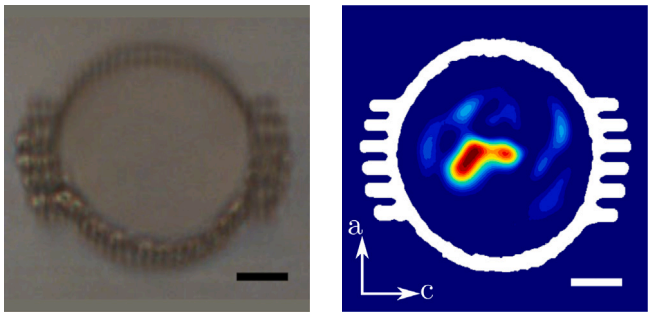

Fig. 2. Microscope image of the cross section of the waveguide (left) and confined mode at 633 nm with the waveguide profile superimposed (right). Both scale bars correspond to 10 µm.

Ti:Sapphire laser system (Spitfire, Spectra Physics). This system emits pulses with a temporal duration of 60 fs, a central wavelength of 800 nm, at a repetition rate of 5 kHz, that are focused in the sample by a 40× microscope objective, after power reduction. The waveguide analyzed in this work is an optimized circular depressed-index cladding structure with a diameter of 40 µm, that consists of multiple parallel damage tracks produced by 70 nJ pulses while scanning the sample at a speed of 0.6 mm/s. The waveguide was inscribed at a depth of about 100 µm below the crystal facet. For more details see Ref. [20].

3. Waveguide characterization

To measure the waveguide propagation losses, we coupled a HeNe laser beam in the waveguide and measured the output power. The ratio between the output power and the incident power is composed by coupling and propagation losses and can be used to set an upper limit for the second contribution. In all the coupling experiments, an Olympus PLN20× microscope objective (N.A. of 0.4) was used as collection optics and both coupling and collection optics were mounted on two independent 3-axis precision translation stages (THORLABS MBT616D/M). The obtained value for the HeNe laser beam is 0.2 dB/cm and it is comparable with the values obtained in femtosecond-laser written waveguides fabricated in fluorides [19,28]. By placing a CCD camera in the conjugate plane of the output facet, we imaged the near field profile of the guided beam. The waveguide shows confinement at 633 nm only for π-polarized light, as already demonstrated by other waveguides realized in birefringent fluorides [16,19]. The intensity profiles are reported, together with an image of the cross section of the waveguide, in Fig. 2. In addition, we estimated the numerical aperture of the waveguide by measuring the divergence of the 633 nm beam exiting from the waveguide. From this measurement, it is possible to roughly estimate the refractive index change in the irradiated area [8]. The obtained value for the numerical aperture is 0.03 and the corresponding refractive index change is $\Delta n = -3 \cdot 10^{-4}$.

We also performed the transmission measurements by using a Cobolt MLD 405 nm, a diode laser emitting a high-quality beam (M^2 = 1.1). The only polarization confined at this wavelength is π polarization. The corresponding limit for the propagation losses is 0.6 dB/cm. We selected 633 nm and 405 nm as test wavelengths since Pr ions do not absorb these frequencies and it is possible to evaluate the contribution of propagation losses neglecting the dopant absorption. The best results at both wavelengths were obtained by using a 30 mm-focal length aspherical lens as coupling lens.

The chosen pump source for the laser experiment is a commercial InGaN-based laser diode tuned to emit at 444 nm. The diode has a maximum output power of 4 W and values of M^2 of 20 and 1.7 for the two principal axes of the beam. The beam was driven to the cavity with a collimator and a couple of cylindrical lenses, used to compensate the beam astigmatism. A half-wavelength plate was used to adjust the beam

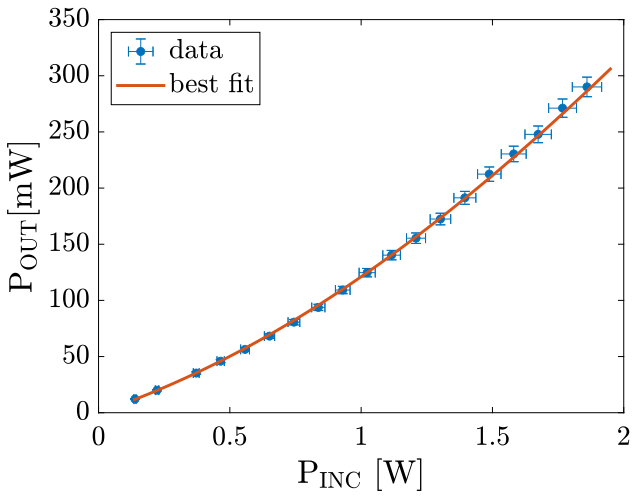

Fig. 3. Residual pump power exiting from the waveguide, measured under non-lasing condition, as a function of the incident power for π-polarized pump light.

polarization and a variable attenuator was employed to control the pump power. The maximum pump power available before the focusing lens was 2.45 W. Due to the saturation of pump absorption [8], it is possible to isolate the contribution of the coupling efficiency from the effect of dopant absorption, as reported in [20]. The best coupling efficiency was achieved employing an aspherical lens of 30 mm focal length, reaching a value of 38%. Data showing the saturation of pump absorption are reported in Fig. 3, together with the best fit used to estimate the coupling efficiency.

By using this coupling optics, the beam diameter was 60 μm in the direction parallel to the *c* axis (M^2 of 20) and 40 μm in the direction parallel to *a* axis (M^2 of 1.7). Since it is possible to measure the coupling efficiency, both the slope efficiencies $\eta_c = \frac{dP_{OUT}}{dP_C}$ and the values of threshold power will be given as a function of the coupled power (P_C).

4. Laser experiments

4.1. Laser system

To test the thermal robustness of the waveguide laser, we built a custom made sample holder. The system was composed by three different parts: a copper radiator (RAD), designed to operate as stabilized heat sink by the use of thermally stabilized water flow, a thermoelectric cooler (TEC), used to stabilize and control the sample holder temperature, and a copper sample holder composed by two copper blocks. The first block (BLOCK 1) has structural function and is connected to the TEC. A hole was made in the side of the holder to insert a thermocouple and measure the temperature slightly under the surface in contact with the crystal. The second one (BLOCK 2) is connected to the first through a copper braid and has the function of locking the sample and improve the crystals temperature control. A second thermocouple was inserted in BLOCK 2 to check the efficiency of the braid. The crystal was inserted between the two copper blocks and an indium foil (measured thickness of 50 μm) was inserted between the copper and LLF to improve the heat exchange. The TEC current was controlled by a custom-made driver capable to stabilize the temperature within less than 0.1 °C. We realized two different configurations. In configuration A, we placed the waveguide facet in contact with BLOCK 1, so as to have about 100 μm of LLF between the waveguide and the temperature reference. Configuration B differs from configuration A for a rotation of the sample around the waveguide axis. The waveguide facet is in contact with BLOCK 2 and about 4 mm of LLF separate the waveguide from BLOCK 1. In this configuration, the larger distance between the waveguide and the TEC leads to a less efficient heat dissipation from the waveguide core and, consequently, to a higher operation temperature. . A schematic representation of the two configurations is reported in Fig. 4.

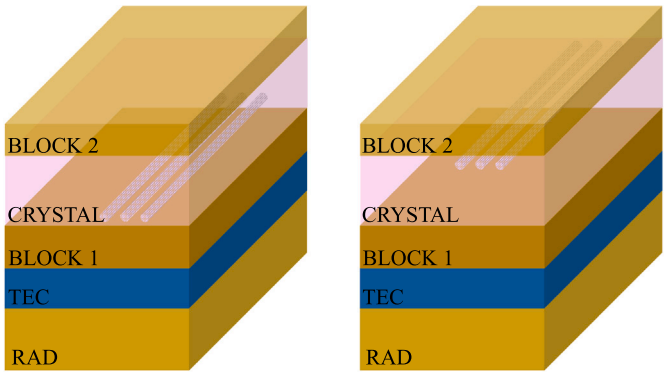

(a) Configuration A. (b) Configuration B.

Fig. 4. Schematic representation of the two configurations studied in this work. The waveguide is represented as a red line. TEC is the thermoelectric cooler while RAD stands for radiator.

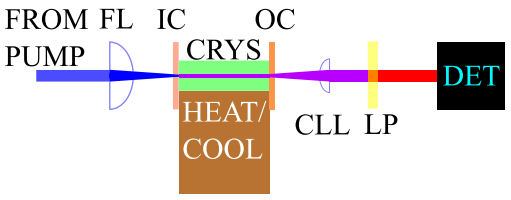

Fig. 5. Schematic representation of the laser cavity. Abbreviations; FL focusing lens, IC input coupler, CRYS crystal, OC output coupler, CLL collection lens, LP long-pass filter, DET instrument for beam analysis. HEAT/COOL represents the thermally stabilized sample holder, described in detail in Fig. 4.

The laser cavity was built by using two plane mirrors, a configuration allowed by the lateral confinement given by the presence of the waveguide. We mounted each mirror in a two axes mirror mount, screwed on a custom made 3D translation stage, that allows to approach the mirror at a short distance from the crystal facet (less than 0.1 mm). The input coupler is highly reflective both at 604 nm (T = 0.1%) and at 721 nm (T ≤ 0.001%) and will be common to all experiments while two different output couplers were used to study the two aforementioned lines. The first one possesses an extraction of 16% at 604 nm and 71% at 721 nm, and it is employed for the analysis of the orange transition. The second one is dedicated to the operation of the 721 nm laser and its extraction at the laser wavelength is 46% while transmitting 96% of the incident light at 604 nm in order to suppress parasitic lasing at this wavelength. Laser radiation was collected by an aspherical lens of 20 mm focal length and a dielectric filter was used to remove the residual pump. A schematic representation of the laser cavity is reported in Fig. 5. During all experiments, the laser spectrum was monitored with a QEpro spectrometer (resolution of about 1 nm).

4.2. Numerical simulations

We simulated the temperature profile inside the waveguide by using COMSOL Multiphysic simulation software, in particular the Heat Transfer Module.

We assumed that the heat source is given by the pump beam which is divided in two components, the coupled one and the scattered one. The coupled one is described as a uniform circular source with a diameter equal to the waveguide diameter (40 μm) and an intensity that exponentially decays as the distance from the input facet is increased.

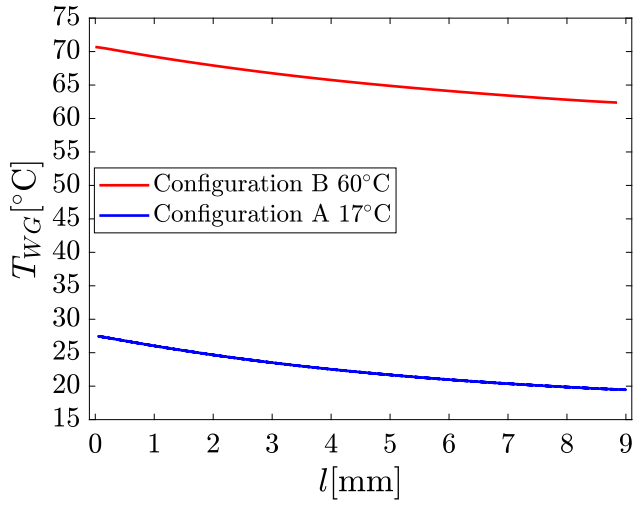

Fig. 6. Simulation of the temperature in the waveguide core, as a function of the distance from the input facet, for configuration A with the sample holder set to 17 °C and for configuration B with a sample holder temperature of 60 °C.

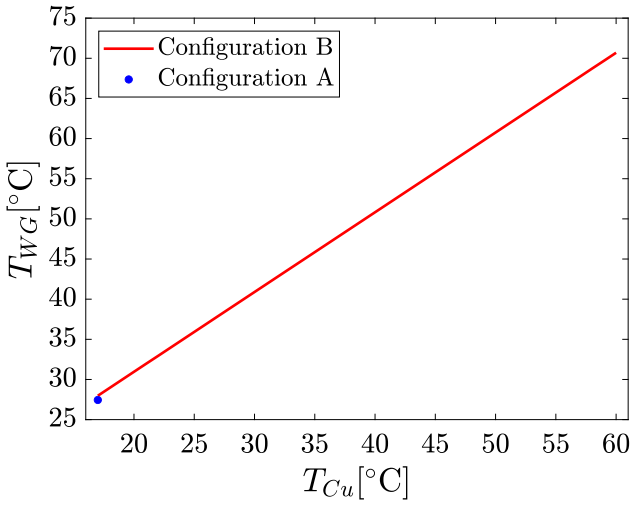

Fig. 7. Maximum value of the core temperature in configuration A and in configuration B as a function of the sample holder temperature.

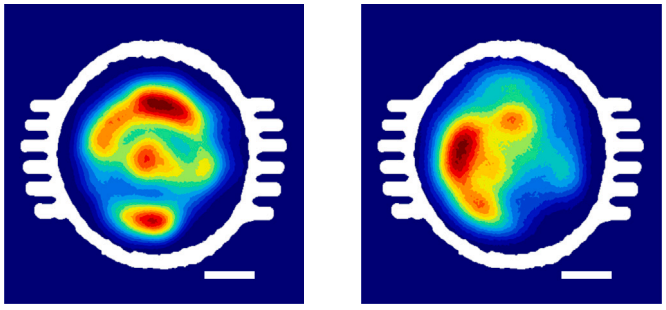

Fig. 8. Intensity profiles of the 604 nm (left) and 721 nm (right) laser emissions, collected at maximum output power in configuration A.

The intensity of this source at the input facet is given by the product of the total power times the coupling efficiency of the pump beam, divided by the waveguide cross section. The estimated intensity at the input facet is equal to 66 kW/cm^2. The remaining scattered pump radiation is taken into account as a heat source that is uniform in the transverse direction of the crystal and with an intensity that decays exponentially in the longitudinal one. For the numerical simulation, we employed the values for the thermomechanical properties of LLF reported in [25]. Four of the six facets of the crystal (the input one, the output one, and the two side ones) exchange heat directly in air, whose temperature was set to 20 °C for all the simulations. For the numerical simulations, we set the heat exchange coefficient between LLF and air equal to 8 W/(m^2 K), the typical value for air-glass interface. To check the robustness of this hypothesis, we increased this coefficient up to 1 kW/(m^2 K), observing a variation in the estimated temperature of the waveguide core lower than 1 °C. To describe the effect of the indium foil, we set an effective interface conductance between copper and LLF equal to 2 MW/m^2 K, the one given by an indium foil of 50 μm thickness. The interface conductance between indium and LLF was assumed equal to 100 MW/m^2 K, that is the one between copper and sapphire, reported in [29]. Due to its higher value, its contribution is negligible with respect to the indium one. To check the effect of these assumptions, we modified the effective interface conductance between 0.2 MW/m^2 K and 100 MW/m^2 K, observing a variation of the core temperature within 1 °C.

We simulated the temperature of the system in configuration A, setting the sample holder temperature at 17 °C. The maximum temperature reached in the waveguide core is about 27 °C, achieved at the input facet. The temperature profile along the core axis is shown in Fig. 6. For configuration B, we performed simulations varying the sample holder temperature from 17 °C to 60 °C. The temperature profile of the waveguide core in configuration B, for a sample holder temperature of 60 °C, is shown in Fig. 6 for comparison with configuration A. The maximum core temperature for each sample holder temperature is reported in Fig. 7. This value has been observed next to the pump input facet. According to the numerical simulations the maximum core temperature is about 70 °C for a 60 °C sample holder temperature.

4.3. Laser results

During the laser experiments, we reproduced the geometries analyzed with the numerical simulations. The first geometry we built is configuration A, already reported in [22], studying the laser performance both at 604 nm and at 721 nm. For the orange transition, we achieved a maximum output power of 275 mW, a slope efficiency of 40% and a threshold power of 110 mW (extraction of the output coupler equal to 16%), while for the 721 nm transition we demonstrated a maximum output power of 310 mW, a slope efficiency of 50% and a threshold power of 170 mW, by using an output coupler with a transmission of 46%. The modal profiles of the two laser emissions, collected at maximum output power, are reported in Fig. 8.

For each laser wavelength, we built configuration B, initially setting the temperature of the sample holder to 17 °C and then we rose the temperature up to 60 °C, measuring the output power at maximum pump power, as a function of the sample holder temperature. We observed variation in the output power of a few milliwatt for both wavelengths, demonstrating the possibility of the laser to operate in thermally severe conditions without being affected in terms of output power. We also checked the temperature reached by the system when dissipating passively in air, by disabling the stabilization system and interrupting the water flux in the radiator. In this condition, the sample holder reached a temperature of about 40 °C. No variation of the output power was observed when the crystal was passively cooled for both wavelengths. The values of output power as a function of the sample holder temperature are reported in Fig. 9 for both wavelengths, together with the values of output power achieved in the reference configuration. In addition, we collected the dependence of the output power on the pump power when the sample holder temperature was set at 60 °C. When operating at 604 nm, the laser demonstrates a maximum output power of 277 mW, a slope efficiency of 41%, and a threshold

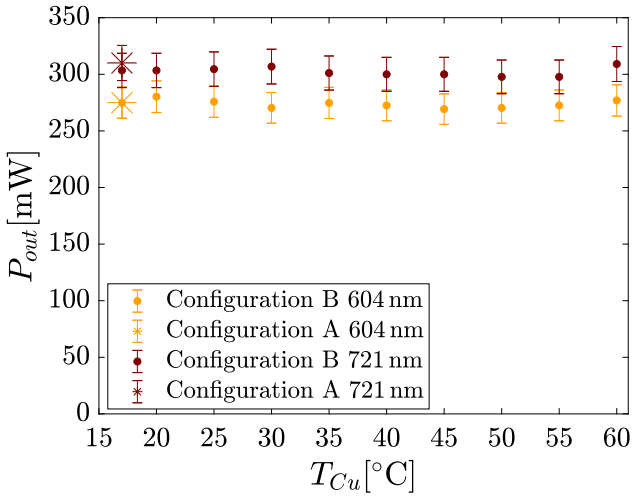

Fig. 9. Output power at maximum pump power in configuration B, as a function of the sample holder temperature. Maximum output power in configuration A is also reported.

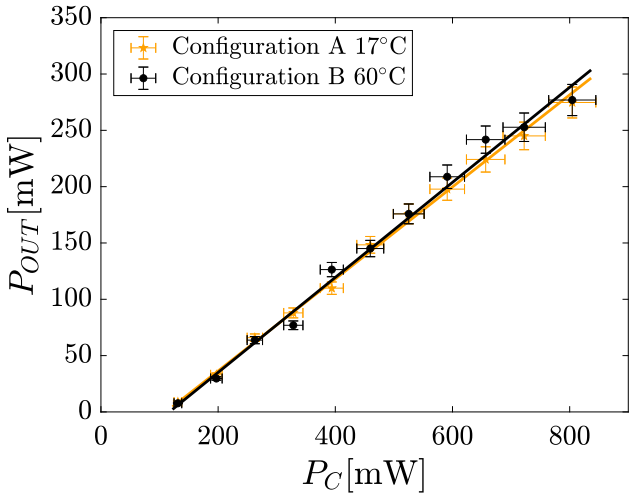

Fig. 10. Output power as a function of the coupled power for the 604 nm waveguide laser, both for configuration A and for configuration B with the sample holder temperature set to 60 °C.

Table 1
Comparison between the laser results achieved in configuration A and in configuration B. λ is the laser wavelength, C is the configuration, T_{Cu} is the sample holder temperature, η_c is the slope efficiency, P_{THR} is the threshold power, and P_{MAX} is the maximum output power.

λ [nm]	C	T_{Cu} [°C]	η_c [%]	P_{THR} [mW]	P_{MAX} [mW]
604	A	17	40	110	275
	B	60	41	115	277
721	A	17	50	170	310
	B	60	51	175	310

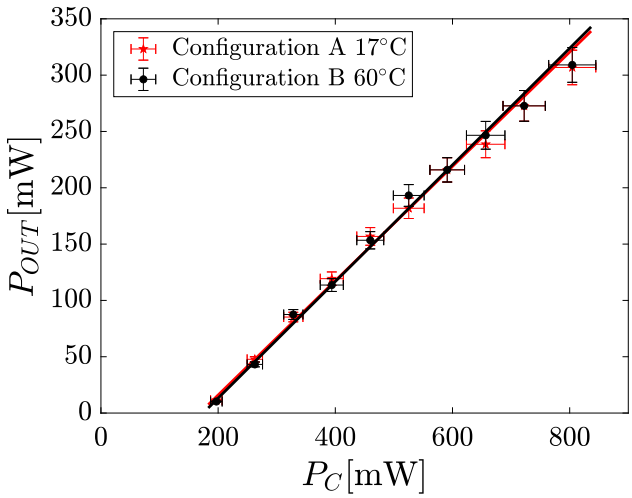

Fig. 11. Output power as a function of the coupled power for the 721 nm waveguide laser, both for configuration A and for configuration B with the sample holder temperature set to 60 °C.

power of 115 mW. Concerning the 721 nm emission, a maximum output power of 310 nm, a slope efficiency of 51% and a threshold power of 175 mW. No difference is present between configuration A and configuration B at maximum temperature. This demonstrates the possibility of operating the waveguide laser in high temperature condition without affecting the bulk-level slope efficiencies reported [13]. Data and best fit for 604 nm line are reported in Fig. 10 while those for the deep red emission are shown in Fig. 11. All the results achieved in configuration B for a sample holder temperature of 60 °C are summarized in Table 1, compared with those reported in configuration A for a holder temperature of 17 °C.

In the end, we checked the stability of the laser system in configuration B at 60 °C and maximum pump power by measuring the output power for 30 min. We observed fluctuations in the output power of about 10% of the maximum value reachable for both wavelengths. We ascribed this effect to the mechanical adjustments of the mirror holders, which are not actively stabilized, that affect the round trip losses, resulting in fluctuations of the output power. The signature of this effect can be found by intentionally increasing the round trip losses. In this way the contribution to the round trip losses given by these adjustments will be negligible with respect to the total and the laser will result more stable. To experimentally implement this condition, we increased the air gap between the output coupler and the crystal facet. With this procedure it is possible to modify the round trip losses, without affecting the pump coupling and, consequently, the thermal load on the system. We repeated the measurements for two different values of output power for each wavelength. By increasing the round trip losses, the fluctuations are reduced within a few percent of the output power, confirming the mechanical origin of the instability. The data collected for the 604 nm laser are reported in Fig. 12, while those for the 721 nm laser are in Fig. 13. Since the output power instability is attributed to the adjustments of the cavity structure, this effect is completely negligible in the perspective of a monolithic laser cavity made by the deposition of a dielectric coating on the crystal facets.

5. Conclusion

In conclusion, we demonstrated the possibility of operating a femtosecond-laser-written waveguide laser in thermally severe conditions, maintaining output powers equal to those achieved for a cooled active medium and bulk-level slope efficiencies, both for the 604 nm the 721 nm transitions. The values of output power here reported are the highest among all diode-pumped Pr-based waveguide lasers [22]. By numerical simulations, we estimated that the waveguide core reaches a temperature of 70 °C, without affecting the guiding properties and the laser performance. In the end, we checked the stability of the device in high temperature conditions, observing fluctuations of less than 10% of the output power, attributed to the mechanical relaxation of the mirror holder system. This opens the door to a further power scaling of the device and to the realization of a passively cooled monolithic waveguide lasers made by the deposition of a dielectric coating on the input and output facets of the crystal. Such a compact and lightweight platform could be the base for aerospace-oriented metrological lasers.

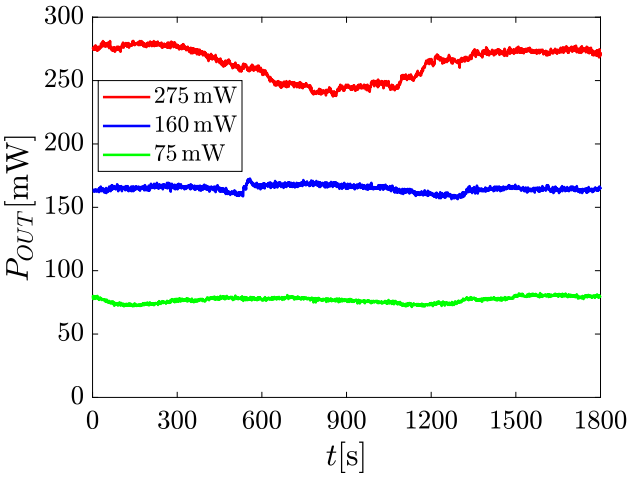

Fig. 12. Output power as a function of time for the 604 nm waveguide laser in configuration B. The sample holder temperature was 60 °C. In the legend the output power at the beginning of the measurement is reported.

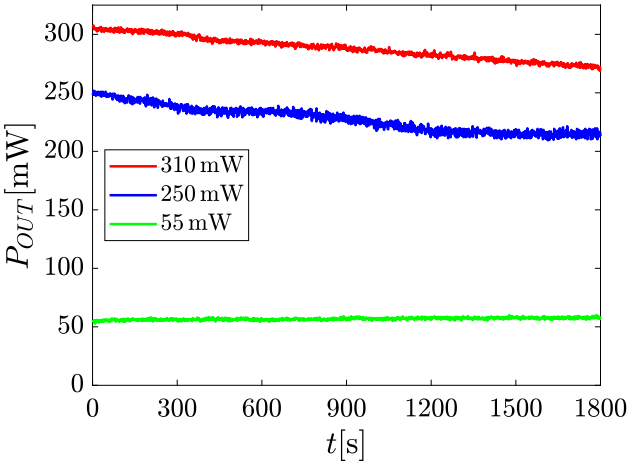

Fig. 13. Output power as a function of time for the 721 nm waveguide laser in configuration B. The sample holder temperature was 60 °C. In the legend the output power at the beginning of the measurement is reported.

Funding

Ministerio de Ciencia, Innovación y Universidades, Spain (PID2020-119818).

CRediT authorship contribution statement

Davide Baiocco: Writing – review & editing, Writing – original draft, Investigation. **Ignacio Lopez-Quintas:** Writing – review & editing, Writing – original draft, Investigation. **Javier R. Vázquez de Aldana:** Writing – review & editing, Writing – original draft, Investigation. **Mauro Tonelli:** Writing – review & editing, Writing – original draft, Investigation. **Alessandro Tredicucci:** Writing – review & editing, Writing – original draft, Investigation.

Declaration of competing interest

The authors declare that they have no known competing financial interests or personal relationships that could have appeared to influence the work reported in this paper.

Data availability

Data will be made available on request.

References

[1] K.M. Davis, K. Miura, N. Sugimoto, K. Hirao, Writing waveguides in glass with a femtosecond laser, Opt. Lett. 21 (21) (1996) 1729–1731, http://dx.doi.org/10.1364/OL.21.001729, URL http://opg.optica.org/ol/abstract.cfm?URI=ol-21-21-1729.

[2] F. Chen, J.R.V. de Aldana, Direct femtosecond laser writing of optical waveguides in dielectrics, in: Laser Micro-Nano-Manufacturing and 3D Microprinting, Springer International Publishing, Cham, 2020, pp. 185–210, http://dx.doi.org/10.1007/978-3-030-59313-1_6.

[3] R. Matthey, C. Affolderbach, G. Mileti, Methods and evaluation of frequency aging in distributed-feedback laser diodes for rubidium atomic clocks, Opt. Lett. 36 (17) (2011) 3311–3313, http://dx.doi.org/10.1364/OL.36.003311, URL http://opg.optica.org/ol/abstract.cfm?URI=ol-36-17-3311.

[4] B. Ayevi, Y. Morova, M. Tonelli, A. Sennaroglu, Er^{3+};:$YLiF_4$ channeled waveguide laser near 2.7-2.8 μm fabricated by femtosecond laser inscription, Opt. Lett. 49 (4) (2024) 1017–1020, http://dx.doi.org/10.1364/OL.515648, URL https://opg.optica.org/ol/abstract.cfm?URI=ol-49-4-1017.

[5] A.G. Okhrimchuk, A.V. Shestakov, I. Khrushchev, J. Mitchell, Depressed cladding, buried waveguide laser formed in a YAG:Nd^{3+} crystal by femtosecond laser writing, Opt. Lett. 30 (17) (2005) 2248–2250, http://dx.doi.org/10.1364/OL.30.002248, URL http://opg.optica.org/ol/abstract.cfm?URI=ol-30-17-2248.

[6] A. Okhrimchuk, V. Mezentsev, A. Shestakov, I. Bennion, Low loss depressed cladding waveguide inscribed in YAG: Nd single crystal by femtosecond laser pulses, Opt. Express 20 (4) (2012) 3832–3843.

[7] Y. Morova, M. Tonelli, A. Sennaroglu, Fabrication of femtosecond laser written depressed-cladding waveguides in Tm^{3+}:BaY_2F_8 crystal and laser operation near 2μm, Opt. Mater. 126 (2022) 112121, http://dx.doi.org/10.1016/j.optmat.2022.112121, URL https://www.sciencedirect.com/science/article/pii/S0925346722001550.

[8] E. Kifle, P. Loiko, X. Mateos, J.R.V. de Aldana, A. Ródenas, U. Griebner, V. Petrov, M. Aguiló, F. Díaz, Femtosecond-laser-written hexagonal cladding waveguide in Tm:$KLu(WO_4)_2$: μ-Raman study and laser operation, Opt. Mater. Express 7 (12) (2017) 4258–4268, http://dx.doi.org/10.1364/OME.7.004258, URL http://opg.optica.org/ome/abstract.cfm?URI=ome-7-12-4258.

[9] T. Calmano, A.-G. Paschke, S. Müller, C. Kränkel, G. Huber, Curved Yb:YAG waveguide lasers, fabricated by femtosecond laser inscription, Opt. Express 21 (21) (2013) 25501–25508, http://dx.doi.org/10.1364/OE.21.025501, URL http://opg.optica.org/oe/abstract.cfm?URI=oe-21-21-25501.

[10] A. Sottile, E. Damiano, A.D. Lieto, M. Tonelli, Diode-pumped solid-state laser platform for compact and long-lasting strontium-based optical clocks, Opt. Lett. 44 (3) (2019) 594–597, http://dx.doi.org/10.1364/OL.44.000594, URL http://opg.optica.org/ol/abstract.cfm?URI=ol-44-3-594.

[11] Y. Zhang, S. Wang, D. Wang, H. Yu, H. Zhang, Y. Chen, L. Mei, A. Di Lieto, M. Tonelli, J. Wang, Atomic-layer molybdenum sulfide passively modulated green laser pulses, IEEE Photonics Technol. Lett. 28 (2) (2015) 197–200.

[12] C. Kränkel, D.-T. Marzahl, F. Moglia, G. Huber, P.W. Metz, Out of the blue: semiconductor laser pumped visible rare-earth doped lasers, Laser Photonics Rev. 10 (4) (2016) 548–568, http://dx.doi.org/10.1002/lpor.201500290, arXiv:https://onlinelibrary.wiley.com/doi/pdf/10.1002/lpor.201500290. URL https://onlinelibrary.wiley.com/doi/abs/10.1002/lpor.201500290.

[13] H. Tanaka, S. Kalusniak, M. Badtke, M. Demesh, N.V. Kuleshov, F. Kannari, C. Kränkel, Visible solid-state lasers based on Pr^{3+} and Tb^{3+}, Prog. Quantum Electron. 84 (2022) 100411, http://dx.doi.org/10.1016/j.pquantelec.2022.100411, URL https://www.sciencedirect.com/science/article/pii/S0079672722000374.

[14] T. Calmano, J. Siebenmorgen, F. Reichert, M. Fechner, A.-G. Paschke, N.-O. Hansen, K. Petermann, G. Huber, Crystalline Pr:$SrAl_12O_19$ waveguide laser in the visible spectral region, Opt. Lett. 36 (23) (2011) 4620–4622, http://dx.doi.org/10.1364/OL.36.004620, URL http://opg.optica.org/ol/abstract.cfm?URI=ol-36-23-4620.

[15] F. Reichert, T. Calmano, S. Müller, D.-T. Marzahl, P.W. Metz, G. Huber, Efficient visible laser operation of Pr,Mg:$SrAl_12O_19$ channel waveguides, Opt. Lett. 38 (15) (2013) 2698–2701, http://dx.doi.org/10.1364/OL.38.002698, URL http://opg.optica.org/ol/abstract.cfm?URI=ol-38-15-2698.

[16] S. Müller, T. Calmano, P. Metz, N.-O. Hansen, C. Kränkel, G. Huber, Femtosecond-laser-written diode-pumped Pr:$LiYF_4$ waveguide laser, Opt. Lett. 37 (24) (2012) 5223–5225, http://dx.doi.org/10.1364/OL.37.005223, URL http://opg.optica.org/ol/abstract.cfm?URI=ol-37-24-5223.

[17] H. Liu, S. Luo, B. Xu, H. Xu, Z. Cai, M. Hong, P. Wu, Femtosecond-laser micromachined Pr:YLF depressed cladding waveguide: Raman, fluorescence, and laser performance, Opt. Mater. Express 7 (11) (2017) 3990–3997, http://dx.doi.org/10.1364/OME.7.003990, URL http://opg.optica.org/ome/abstract.cfm?URI=ome-7-11-3990.

[18] Y. Ren, Z. Cui, L. Sun, C. Wang, H. Liu, Y. Cai, Laser emission from low-loss cladding waveguides in Pr:YLF by femtosecond laser helical inscription, Chin. Opt. Lett. 20 (12) (2022) 122201, URL https://opg.optica.org/col/abstract.cfm?URI=col-20-12-122201.

[19] D. Baiocco, I. Lopez-Quintas, J.R.V. de Aldana, M. Tonelli, A. Tredicucci, Diode-pumped visible lasing in femtosecond-laser-written Pr:$LiLuF_4$ waveguide, Opt. Lett. 48 (7) (2023) 1734–1737, http://dx.doi.org/10.1364/OL.487318, URL https://opg.optica.org/ol/abstract.cfm?URI=ol-48-7-1734.

[20] D. Baiocco, I. Lopez-Quintas, J. R. Vázquez de Aldana, M. Tonelli, A. Tredicucci, Comparative performance analysis of femtosecond-laser-written diode-pumped Pr:$LiLuF_4$ visible waveguide lasers, Photonics 10 (4) (2023) http://dx.doi.org/10.3390/photonics10040377, URL https://www.mdpi.com/2304-6732/10/4/377.

[21] A. Baillard, P. Loiko, C. Romero, V. Arroyo, J.R.V. de Aldana, M. Fromager, A. Benayad, A. Braud, P. Camy, X. Mateos, Orange surface waveguide laser in Pr:$LiYF_4$ produced by a femtosecond laser writing, Opt. Lett. 48 (23) (2023) 6212–6215, http://dx.doi.org/10.1364/OL.507073, URL https://opg.optica.org/ol/abstract.cfm?URI=ol-48-23-6212.

[22] D. Baiocco, I. Lopez-Quintas, J.R.V. de Aldana, M. Tonelli, A. Tredicucci, High efficiency diode-pumped Pr:$LiLuF_4$ visible lasers in femtosecond-laser-written waveguides, Opt. Express 32 (6) (2024) 9767–9776, http://dx.doi.org/10.1364/OE.516789, URL https://opg.optica.org/oe/abstract.cfm?URI=oe-32-6-9767.

[23] Q. Yang, H. Liu, S. He, Q. Tian, B. Xu, P. Wu, Circular cladding waveguides in Pr: YAG fabricated by femtosecond laser inscription: Raman, luminescence properties and guiding performance, Opto-Electron. Adv. 4 (2) (2021) 200005, 200005–1.

[24] P.W. Metz, F. Reichert, F. Moglia, S. Müller, D.-T. Marzahl, C. Kränkel, G. Huber, High-power red, orange, and green Pr3+:LiYF4 lasers, Opt. Lett. 39 (11) (2014) 3193–3196, http://dx.doi.org/10.1364/OL.39.003193, URL https://opg.optica.org/ol/abstract.cfm?URI=ol-39-11-3193.

[25] R.L. Aggarwal, D.J. Ripin, J.R. Ochoa, T.Y. Fan, Measurement of thermo-optic properties of $Y_3Al_5O_{12}$, $Lu_3Al_5O_{12}$, $YAlO_3$, $LiYF_4$, $LiLuF_4$, BaY_2F_8, $KGd(WO_4)_2$, and $KY(WO_4)_2$ laser crystals in the 80–300 K temperature range, J. Appl. Phys. 98 (10) (2005) 103514, http://dx.doi.org/10.1063/1.2128696, arXiv:https://doi.org/10.1063/1.2128696.

[26] A.A. Kaminskii, K. ichi Ueda, N. Uehara, New laser-diode-pumped CW laser based on Nd^{3+}-ion-doped tetragonal $LiLuF_4$ crystal, Japan. J. Appl. Phys. 32 (Part 2, No. 4B) (1993) L586–L588, http://dx.doi.org/10.1143/jjap.32.l586.

[27] F. Cornacchia, A. Richter, E. Heumann, G. Huber, D. Parisi, M. Tonelli, Visible laser emission of solid state pumped $LiLuF_4$:Pr^{3+}, Opt. Express 15 (3) (2007) 992–1002, http://dx.doi.org/10.1364/OE.15.000992, URL http://opg.optica.org/oe/abstract.cfm?URI=oe-15-3-992.

[28] Y. Morova, B. Morova, H. Jahangiri, I. Baylam, A. Di Lieto, G. Cittadino, E. Damiano, M. Tonelli, A. Sennaroglu, Femtosecond laser written continuous-wave Nd^{3+}:BaY_2F_8 waveguide laser at 1.3 μm, Opt. Mater. 134 (2022) 113199, http://dx.doi.org/10.1016/j.optmat.2022.113199, URL https://www.sciencedirect.com/science/article/pii/S0925346722012368.

[29] B.C. Gundrum, D.G. Cahill, R.S. Averback, Thermal conductance of metal-metal interfaces, Phys. Rev. B 72 (2005) 245426, http://dx.doi.org/10.1103/PhysRevB.72.245426, URL https://link.aps.org/doi/10.1103/PhysRevB.72.245426.